Inorganic Chemistry
Article
pubs.acs.org/IC

Theoretical Modeling of Spin Crossover in Metal–Organic Frameworks: $[Fe(pz)_2Pt(CN)_4]$ as a Case Study

Jordi Cirera, Volodymyr Babin, and Francesco Paesani*

Department of Chemistry and Biochemistry, University of California San Diego, La Jolla, California 92093-0314, United States

S Supporting Information

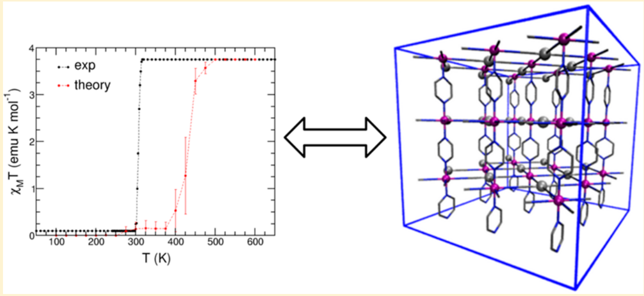

ABSTRACT: Metal–organic frameworks (MOFs) with spin-crossover behavior are promising materials for applications in memory storage and sensing devices. A key parameter that characterizes these materials is the transition temperature $T_{1/2}$, defined as the temperature with equal populations of low-spin and high-spin species. In this study, we describe the development, implementation, and application of a novel hybrid Monte Carlo/molecular dynamics method that builds upon the Ligand Field Molecular Mechanics approach and enables the modeling of spin-crossover properties in bulk materials. The new methodology is applied to the study of a spin-crossover MOF with molecular formula $[Fe(pz)_2Pt(CN)_4]$ (pz = pyrazine). The total magnetic moment of the material is determined as a function of the temperature from direct calculations of the relative equilibrium populations of both low-spin and high-spin states of each Fe(II) center of the framework. The $T_{1/2}$ value, calculated from the temperature dependence of the magnetization curve, is in good agreement with the available experimental data. A comparison between the spin-crossover behavior of the isolated secondary building block of the framework and the bulk material is presented, which reveals the origin of the different spin-crossover properties of the isolated molecular system and corresponding MOF structure.

1. INTRODUCTION

Metal–organic frameworks (MOFs) are a relatively new class of porous materials that have attracted considerable interest due to their potential technological applications.[1−3] Although coordination networks have been known for a long time,[4] it was not until 1994 that the acronym MOF was introduced to describe this type of hybrid organic–inorganic materials.[5] Since then, the volume of publications, monographic studies, and specialized books dedicated to MOFs has continued to grow.[6−10] MOFs are constructed by connecting metal ions or clusters (often referred to as secondary building units or SBUs) with organic linkers to form one-, two- or three-dimensional porous structures with high surface areas. This particular property makes MOFs promising candidates for hydrogen and methane storage, carbon capture, compound separation, and purification processes.[2,11−13] Unlike other porous materials, such as zeolites, MOFs are highly designable, which allows not only the size and shape but also the physicochemical properties of the framework to be tuned for specific applications. Pre-synthetic,[14] postsynthetic,[15,16] and both metal- and ligand-exchange[17] strategies have been shown to be viable routes for the modification of the framework properties.

The incorporation of open-shell metal centers such as Fe(II) and Co(II) into the frameworks results in MOFs that can display spin-crossover (SCO) behavior.[1−3,18,19] When transition metals with electron configurations d^4 to d^7 are placed in a ligand field, the degeneracy of the d orbitals is removed, and different spin states become accessible. For example, in octahedral coordination environments (such as those usually provided by MOFs), the d orbital manifold splits into two sets of orbitals, namely, the nonbonding t_{2g} and the antibonding e_g sets. Depending on the energy gap between the two sets of orbitals, the system can exist in two possible spin states, the low-spin (LS) and the high-spin (HS) state. If the energy gap between the t_{2g} and e_g sets is comparable to the pairing energy, SCO occurs in response to external perturbations driven by temperature gradients, pressure fluctuations, or light irradiation.[18] Since entropic effects favor the HS state, the LS state is found at relatively lower temperatures.

The combination of large surface areas and high framework tunability makes SCO MOFs (or SCOFs) promising multi-functional materials for potential applications in nanoscale memory devices and sensors.[9,20−22] In this regard, SCO transitions in MOFs are accompanied by distinct changes in the physicochemical properties of the frameworks (e.g., color, magnetism, and structure). Importantly, it was shown that the range of temperatures associated with SCO transitions in MOFs can be modulated by the adsorption of guest molecules.[21,23−26] Remarkable examples of this behavior are provided by the $[Fe(pz)_2Pt(CN)_4]$ MOF, which displays bidirectional chemo-switching of spin state upon adsorption of different guest molecules. While the SCO transition in the empty MOF occurs at ~290 K, it was found that the adsorption

Received: June 26, 2014
Published: October 1, 2014

of protic solvents (e.g., alcohols and water) and aromatic molecules (e.g., benzene and pyridine) stabilizes the HS state, shifting the transition to lower temperatures. By contrast, CS_2 molecules adsorbed in the pores stabilize the LS state. Small molecules such as CO_2 and N_2 were found not to affect the SCO properties. It was also shown that the $[Fe(pz)_2Pt(CN)_4]$ MOF exhibits "memory" response, being able to retain a given spin state upon guest desorption.[21]

Although there seems to be a correlation between the SCO transition and the dielectric constant of the guest molecules,[23] the modulation of the SCO behavior upon guest adsorption at the molecular level remains poorly understood. In this context, the development and application of accurate theoretical/computational methodologies for simulations of SCO phenomena in large molecular systems is of particular relevance since it can provide fundamental insights that are important for the rational design of multifunctional materials. Electronic structure methods have been applied to calculate thermodynamic quantities and relative electronic energies in molecular SCO systems with varying degrees of success.[27−30] However, these reduced molecular models cannot retrieve cooperative or crystal-packing effects crucial in determining the overall shape of the magnetization curve in crystalline materials.[1,18]

In this study, we describe the development, implementation, and application of a novel hybrid Monte Carlo/molecular dynamics (MC/MD) method that builds upon the ligand field molecular mechanics (LFMM) approach[31−35] and enables modeling of SCO properties in bulk materials. Here, we examine the SCO behavior of the $[Fe(pz)_2Pt(CN)_4]$ MOF through direct calculations of the relative populations of LS and HS states of each metal center of the framework at different temperatures. The agreement between the calculated and measured transition temperatures provides evidence for the accuracy of our hybrid MC/MD approach. The article is organized as follows: in Section 2, we provide the theoretical background of the LFMM approach and describe our extension to SCO materials in combination with the development of ab initio-based ligand-field force fields (LF-FFs). The validation of our LFMM approach is presented in Section 3 along with the discussion of the simulation results for the $[Fe(pz)_2Pt(CN)_4]$ MOF. A brief summary and outlook are given in Section 4.

2. METHODOLOGY

2.1. Ligand Field Molecular Mechanics. The development and application of flexible force fields derived from ab initio data have recently enabled the accurate modeling of structural, thermodynamic, and dynamical properties of MOFs through computer simulations.[27,36−41] In particular, MD simulations carried out with flexible force fields have played an important role in the identification of the physical mechanisms responsible for the so-called "breathing behavior" that is associated with reversible structural deformations that MOFs undergo in response to external stimuli.[27,38,40,41] However, conventional MD approaches employed in refs 27, 38, 40, and 41 assume that each metal center of the framework can only access a single electronic state throughout the entire simulation. Therefore, although quite accurate, these approaches cannot be applied to the study of SCO systems that undergo transitions between multiple spin states as a function of temperature.

The limitations of existing MOF force fields in treating multiple electronic states can be overcome by building upon the ligand field molecular mechanics (LFMM) approach developed by Deeth and coworkers.[31−35] Within LFMM, conventional molecular mechanics (MM) energy expressions are supplemented with an additional term that effectively represents the ligand field stabilization energy (LFSE) arising from the splitting and different occupation of the d orbitals of the metal centers. LFMM thus explicitly includes energy contributions that depend on both the instantaneous coordination geometry and the electronic structure of the metal centers. Since the LFMM method has recently been reviewed in ref 34, only a brief description of the main concepts and specific details relevant to the present application to SCOF materials are discussed in the following.

The LFMM method builds upon the angular overlap model (AOM) proposed by Schaeffer and Jorgensen.[42] AOM approximates the total ligand field potential, V^{LF}, of a generic complex (M = metal and L = ligand) with a sum of localized contributions associated with each M−L bond. As a result, the complex is effectively treated as n M−L diatomic molecules, each with its own σ- and π-bonding properties. V^{LF} includes radial contributions that are specific to the chemical nature of each M−L bond and angular contributions that depend on the geometry of the complex. The radial contributions are represented by the AOM parameters e_λ (with $\lambda = \sigma, \pi, ...$), which, in turn, are expressed as power series of the corresponding inverse bond distances (r)

$$e_\lambda = a_0 + \sum_{k=1} a_k \mathrm{r}^{-k} \tag{1}$$

where a_k are fitting parameters. The AOM parameters e_λ are directly related to the energy gaps between the d-based molecular orbitals and, therefore, depend on the coordination environment of the ML_n complex. For example, in a perfect octahedral environment with six equal σ donor ligands, the energy gap (Δ_{Oh}) between the antibonding (e_g) and nonbonding (t_{2g}) orbitals is given by $\Delta_{Oh} = 3e_\sigma$. Similar expressions can be derived for all other coordination geometries and different ligand combinations.[43,44] The angular contribution to each d-based molecular orbital is expressed in terms of the square of the overlap between the corresponding metal d orbital and a suitable ligand orbital. Within the AOM formalism, the energy of each d-based orbital in a given coordination environment thus depends on all M−L interactions and is expressed in terms of trigonometric functions (F) of the ligand angular coordinates θ and ϕ. The actual energy of each d-based orbital is then obtained from the diagonalization of the 5 × 5 matrix representing the total ligand field potential,

$$\langle \mathrm{d}_i | V^{LF} | \mathrm{d}_j \rangle = \sum_{l}^{N} \sum_{k} F_{ik}^{l} F_{jk}^{l} e_k^{l} \tag{2}$$

Using eq 2, the LFSE contribution is calculated as the sum of the five eigenvalues (w_i) of the V^{LF} matrix weighted by the corresponding occupation number (n_i),

$$\mathrm{LFSE} = \sum_{i=1}^{5} n_i w_i \tag{3}$$

By construction the LFMM method also overcomes the so-called "unique labeling problem" associated with the description of ML_n complexes. This problem arises from the fact that the description of ML_n complexes using conventional force fields needs the use of multiple reference angles for the same L−M−L triad, thus requiring the definition of multiple equilibrium positions and redundant atom labeling schemes.[45] In its original version (available in the DommiMOE software[35]), the LFMM approach has been successfully applied to investigate electronically driven effects on several coordination complexes.[34,46−49]

To enable direct simulations of the SCO properties of bulk materials, we combined the original LFMM approach of refs 31−35 with a Monte Carlo scheme based on the Metropolis acceptance/rejection criterion that is used to model the transitions between different spin states, enabling the direct calculation of the LS and HS equilibrium populations of each metal center. The resulting hybrid MC/MD scheme was then extended to systems with multiple metal centers in periodic boundary conditions. Our MC/MD approach, implemented in a modified version of the DL_POLY Classic software,[50] is designed to describe SCO materials with an arbitrary number of different metal centers, each with its own set of possible spin states. Specifically, for any instantaneous molecular configuration generated throughout an MD trajectory, the energy gap (ΔE) between LS and HS states of each metal center is calculated using the LFMM approach, and the transitions between the two states are allowed with probability $P = \min(1,\exp(-\Delta E/k_BT))$, where k_B is Boltzmann's constant, and T is the temperature. Our specific LFMM implementation also includes the electron−electron repulsion term discussed in ref 35. This term, which in our study is determined from ab initio calculations, primarily affects the properties of the LS state and is necessary for the correct description of the relative energies between the two spin states. Particularly relevant to the characterization of SCOF materials is the ability of performing our hybrid MC/MD simulations in the constant stress−constant temperature (NσT) ensemble, which allows the monitoring of the SCO transitions on each metal center of the framework as a function of both temperature and pressure. This provides a direct connection between the SCO properties and possible structural deformations (e.g., pore size and shape) of the framework. In the following, we will use "MD" to indicate molecular dynamics simulations performed for a system in a specific (either low or high) spin state. By contrast, "MC/MD" will refer to hybrid Monte Carlo/molecular dynamics simulations in which the spin states of the metal centers are allowed to change along the dynamical trajectory.

We validated our specific LFMM implementation via the analysis of a series of $[MCl_4]^{2-}$ complexes (with M = Co, Ni, and Cu), for which complete sets of LFMM parameters are available in the literature.[35] These complexes, in which the metal centers differ in both number of d electrons and spin states, represent a comprehensive test for the accuracy of the LFMM implementation and offer a systematic approach to its validation. The results of our analysis, reported in the Supporting Information, are in excellent agreement with the corresponding values reported in ref 35, and thus validate our implementation.

2.2. Computational Methods. The key quantity for the physical characterization of SCO systems is the transition temperature $T_{1/2}$, defined as the temperature with equal populations of LS and HS species.[18] The ability of predicting $T_{1/2}$ with accuracy plays a central role in the rational design of SCO materials with tailored properties for technological applications.[1,3,20,21,51] The calculation of $T_{1/2}$ is challenging because of the difficulties associated with the accurate determination of the energy gap between the two spin states. Within density functional theory (DFT), several functionals have been proposed for modeling SCO properties. Among them, B3LYP(*), derived from the original B3LYP functional by adjusting the amount of Hartree−Fock exchange to 15%, was shown to provide an accurate description of the relative electronic energies of $[Fe(NH)S_4]L$ (NHS_4 = 2,2-bis(2-mercaptophenylthio)diethylamino, and L = CO, NO^+, PR_3, NH_3, and N_2H_4) and $[Fe(phen)_2(NCS)_2]$ (phen = phenanthroline) complexes.[29,52] The energy gaps between the two spin states was also determined in a series of Fe(II) compounds using DFT models that combine the OPTX[53] exchange functional with the LYP[54] and PBE[55] correlation functionals. More recently, double hybrid functionals have also been used in calculations of the spin-state energetics of different SCO compounds.[56]

In previous studies,[27,28] we showed that the hybrid meta-GGA functional TPSSh[57] correctly reproduces spin-state energy differences in several prototypical SCO systems. In particular, compared to other meta-GGA functionals, TPSSh predicts accurate enthalpy changes associated with SCO transitions in a large number of Fe(II) and Co(II) compounds. More recently, the TPSSh functional has been used to estimate free-energy changes associated with SCO transitions in a family of ligand-driven light-induced spin-change (LD-LISC) complexes with molecular formula $[Fe(stpy)_4(NCX)_2]$ (X = S, Se, or BH_3).[27] The computational methodology proposed in ref 27 has also been applied to the characterization of SCO phenomena in assembled complexes with molecular formula $[Fe(NCX)_2(bpa)_2]_n$ (X = S, Se, and BH_3 and bpa = 1,2-bis(4-pyridyl)ethane).[58] On the basis of the results reported in refs 25 and 26, we used the TPSSh functional in all DFT calculations required for the parametrization of the ab initio-based LF-FFs described in the following section.

All calculations were performed with Gaussian 09 (Rev C.01),[59] using a 10^{-8} convergence criterion for the elements of the density matrix. The fully optimized contracted triple-ζ all-electron Gaussian basis set developed by Ahlrichs and co-workers was employed for all atoms, with the addition of polarization functions for Fe.[60] The Stuttgart/Dresden effective core potential including relativistic effects was used for Pt.[61] A modified version of the DL_POLY_Classic software[50] was used for both MD and hybrid MC/MD calculations. The Merck molecular force field (MMFF94)[62] was used to model the intramolecular interactions of the organic ligands (pyrazine and cyanide ligands). Specific LFMM parametrizations for the interactions between the metal centers and the organic ligands were derived from fits to the TPSSh data. The optimization process was performed using the genetic algorithm.[63] The Lennard-Jones parameters for Pt(II) and Fe(II) where taken from the literature.[64,65]

The LF-FF parameters for the $[Fe(pz)_2Pt(CN)_4]$ MOF were obtained from fits to ab initio data calculated for the individual secondary building units, $[Fe(pz)_2(NC)_4]^{2-}$ and $[Pt(CN)_4]^{2-}$. Neutral models, in which the negative charges were properly balanced, as well as combined models containing both Fe(II) and Pt(II) centers, were also considered for the LF-FF parametrization. However, none of these models is capable of correctly reproducing the geometry of the $[Fe(pz)_2(NC)_4]$ unit found in the actual MOF structure. Our analysis also indicates that the relative energies between the low- and high-spin states of Fe(II) were effectively independent of the choice of the reduced models employed in the LF-FF parametrization. On the basis of these findings, the use of the individual $[Fe(pz)_2(NC)_4]^{2-}$ and $[Pt(CN)_4]^{2-}$ units in the LF-FF parametrization was preferred because these two SBUs provide structural properties in close agreement with the crystallographic data available for the actual MOF.

To realistically reproduce the electrostatic environment found in the neutral $[Fe(pz)_2Pt(CN)_4]$ MOF, the atomic partial charges were determined by performing a natural bond order (NBO) analysis on two extended models, each containing the relevant (geometry-optimized) SBU (see Figure S10 in the Supporting Information). Following ref 66 the electroneutrality in these models was enforced by protonating the terminal CN^- groups. However, effectively identical atomic partial charges were also obtained by balancing the negative charges with Li^+ atoms placed next to the terminals CN^- groups. The unit cell used to construct the MOF structure in periodic boundary conditions is shown in the Supporting Information, Figure S10, along with the complete list of the atom types and corresponding atomic partial charges used in both MD and hybrid MC/MD simulations.

All MD and hybrid MC/MD simulations of the $[Fe(pz)_2(NC)_4]^{2-}$ model were carried out in the canonical (NVT) ensemble using a 500 $Å^3$ simulation box and the direct Coulomb sum for correctly modeling the electrostatic interactions within the isolated system. All 1−2 and 1−3 bonded interactions were excluded from the calculation of the nonbonded interactions. The temperature was maintained using a Nosé−Hoover thermostat with a relaxation time of 1 ps, and the equations of motion were propagated using the velocity-Verlet algorithm with a time step of 1 fs.

All MD and hybrid MC/MD simulations of the $[Fe(pz)_2Pt(CN)_4]$ MOF were carried out for a structure consisting of 2 × 2 × 2 unit cells in periodic boundary conditions. The short-range interactions were truncated at an atom−atom distance of 9.0 Å, and the electrostatic interactions were treated using the smooth particle mesh Ewald method.[67] The simulations were performed in the NσT ensemble, and all properties were calculated by averaging over 5 ns. The temperature and pressure were maintained using Nosé−Hoover thermostats and barostats with relaxation times of 1 and 5 ps, respectively. The equations of motion were propagated according to the velocity−Verlet algorithm with a time step of 1 fs.[67]

3. RESULTS

3.1. Development of ab Initio-Based Ligand Field Force Fields. Among different MOFs reported in the literature, $[Fe(pz)_2Pt(CN)_4]$ has attracted considerable interest because it undergoes the SCO transition, with a small hysteresis of ∼24 K, near room temperature ($T_{1/2,\text{ down}}$ = 285 K and $T_{1/2,\text{ up}}$ = 309 K).[21] Furthermore, it was shown that the magnetic properties of [Fe(pz)$_2$Pt(CN)$_4$] can be controlled at the molecular level through adsorption of chemically and structurally different guest molecules. Specifically, it was found that water, small alcohols, and aromatic molecules with five- and six-membered rings stabilize the HS state, while CS$_2$ stabilizes the LS state.[21] Thiourea was found to widen the hysteresis loop relative to the empty framework from 24 to 64 K.[20] No effects on $T_{1/2}$ were instead observed upon adsorption of small molecules such as O$_2$, N$_2$, and CO$_2$.

Within the LFMM scheme, the molecular modeling of the SCO properties of [Fe(pz)$_2$Pt(CN)$_4$] MOF requires the parametrization of LF-FFs for two different types of metals, Pt(II) (d^8, low-spin S = 0, in silver in Figure 1) and Fe(II) (d^6, low-spin S = 0, and high-spin S = 2, in purple in Figure 1). As mentioned in Section 2, the LF-FFs for both Pt(II) and Fe(II) were derived from fits to TPSSh data obtained for two model systems (Figure 1) mimicking the two inorganic SBUs of the [Fe(pz)$_2$Pt(CN)$_4$] MOF, namely, [Pt(CN)$_4$]$^{2-}$ and [Fe(pz)$_2$(CN)$_4$]$^{2-}$. For each SBU, the reference ab initio data were calculated for 21 equally spaced molecular configurations along the displacement vectors of the corresponding normal modes. Since the SCO transition in the [Fe(pz)$_2$Pt(CN)$_4$] MOF occurs at ∼300 K (∼208 cm^{-1}), only normal modes with frequencies below 500 cm^{-1} were included in the fitting process since the contribution of normal modes with higher frequencies is negligible. The same criterion was also applied to the parametrization of the Pt(II) LF-FF. As a result, 357 reference energies corresponding to the 17 normal modes with associated frequencies below 500 cm^{-1} were calculated for the Pt(II) unit, and 693 reference energies corresponding to 33 normal modes with associated frequencies below 500 cm^{-1} were calculated for each spin state of the Fe(II) unit at the TPSSh/triple-ζ level of theory[27] (see Supporting Information). The TPSSh reference energies were then used to fit all LF-FF parameters describing the bonded interactions between the metal centers and the organic ligands. For each structure sampled along the normal modes, the energies of the d-based molecular orbitals extracted from the TPSSh calculations were used to parametrize all AOM distance-dependent functions (eq 1). All LF-FF parameters for both [Pt(CN)$_4$]$^{2-}$ and [Fe(pz)$_2$(NC)$_4$]$^{2-}$ are listed in Table S7 of the Supporting Information.

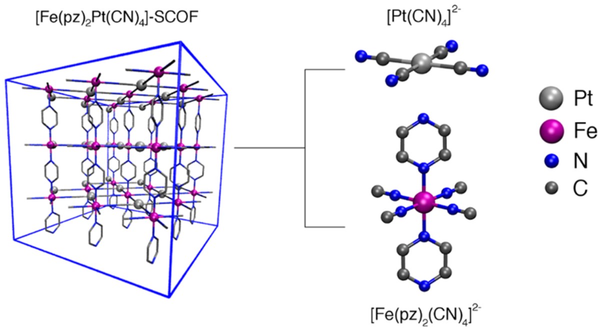

Figure 1. (left) Three-dimensional representation of the [Fe(pz)$_2$Pt(CN)$_4$] MOF. (right) Secondary building units [Pt(CN)$_4$]$^{2-}$ (upper) and [Fe(pz)$_2$(NC)$_4$]$^{2-}$ (lower) used as model systems in the TPSSh/triple-ζ calculations required for the parametrization of the Fe(II) and Pt(II) LF-FFs. All hydrogen atoms are omitted for clarity.

The accuracy of the Pt(II) and Fe(II) LF-FFs was assessed by comparing the LF-FF vibrational frequencies calculated for the two MOF building units of Figure 1 with the corresponding TPSSh reference values. The LF-FF minimum-energy structure of the [Pt(CN)$_4$]$^{2-}$ system, which exists only in the LS state (S = 0), is shown in Figure 2a along with the comparison between the corresponding LF-FF and TPSSh vibrational frequencies (Figure 2b). The ab initio-based LF-FF, which accounts for both σ and π interactions and d/s mixing, correctly reproduces the square planar geometry expected for a low-spin d^8 metal center. Both LF-FF bond lengths (Table 1) and harmonic frequencies (Figure 2b) are in good agreement with the corresponding TPSSh results, with a root-mean square error (RMSE) of 4.67 cm^{-1} per normal mode with vibrational frequency below 500 cm^{-1}. The complete list of the harmonic frequencies for the [Pt(CN)$_4$]$^{2-}$ molecule is reported in the Supporting Information (Table S2).

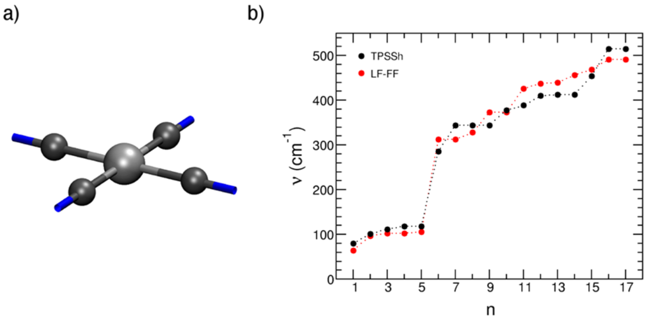

Figure 2. (a) LF-FF optimized geometry of the [Pt(CN)$_4$]$^{2-}$ subunit. All atoms whose interactions are described through the LFMM parametrization are shown explicitly. (b) Comparison between the TPSSh (black) and the LF-FF (red) harmonic frequencies below 500 cm^{-1} calculated for the [Pt(CN)$_4$]$^{2-}$ subunit (n is the normal-mode index).

A similar procedure was adopted for the parametrization of the LS and HS LF-FFs for the [Fe(pz)$_2$(NC)$_4$]$^{2-}$ subunit. As mentioned above, in this case, the inclusion of an explicit electron−electron repulsion term was found to be necessary for accurately reproducing the energy gap between the potential energy surfaces associated with the two spin states. The electron−electron repulsion term was specifically fit to reproduce the energy difference along the TPSSh minimum energy path that interpolates from the optimized LS to HS geometries of the [Fe(pz)$_2$(NC)$_4$]$^{2-}$ subunit. As shown in Figure 3, the LF-FF results accurately reproduce the potential energy curves obtained at the TPSSh/triple-ζ level of theory for both LS and HS states. The LF-FF energy difference between the geometry-optimized LS and HS states is 10.33 kcal/mol, which compares quite favorably with the TPSSh value of 10.62 kcal/mol.

The LF-FF harmonic frequencies of the [Fe(pz)$_2$(NC)$_4$]$^{2-}$ subunit are in good agreement with the corresponding TPSSh values (Figure 4), with RMSEs of 2.85 and 2.07 cm^{-1} per normal mode with frequency below 500 cm^{-1} for LS and HS states, respectively. (The complete list of the harmonic frequencies is reported in Tables S3 and S4 of the Supporting Information). The comparison between the LF-FF and TPSSh results for several structural parameters of the geometry-optimized [Fe(pz)$_2$(NC)$_4$]$^{2-}$ subunit is reported in Table 1. As expected, the bond lengths in the HS state are relatively longer due to the occupation of antibonding orbitals (Figure S9 in the

Table 1. Optimized Bond Lengths and Bond Angles at DFT and LFMM Levels for $[Pt(CN)_4]^{2-}$ and $[Fe(pz)_2(NC)_4]^{2-}$

	M−L (LF-FF) (Å)	M−L (DFT) (Å)	L−M−L (LF-FF) (deg)	L−M−L (DFT) (deg)
Pt-CN(d^8, S=0)	2.01	2.02	90.0	90.0
Fe-pz(d^6, S=0)	1.94	1.94	90.0	90.0
Fe-NC(d^6, S=0)	1.93	1.96	90.0	90.0
Fe-pz(d^6, S=2)	2.17	2.16	90.0	90.0
Fe-NC(d^6, S=2)	2.16	2.14	90.0	90.0

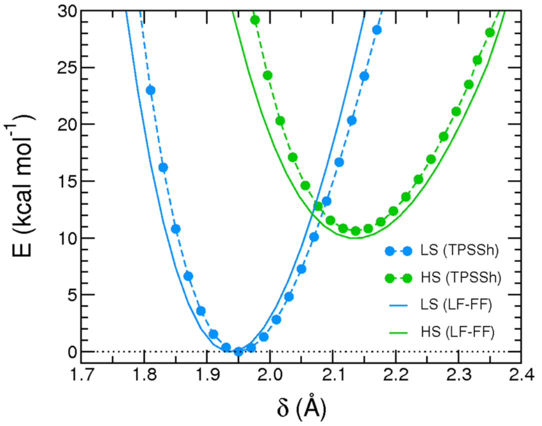

Figure 3. Potential energy curves for the LS (blue) and HS (green) states along the TPSSh minimum energy path interpolating between the equilibrium geometries of the two different spin states. The distance reported on the x-axis corresponds to the average value of the six M−L bonds. The TPSSh/triple-ζ and LF-FF results are shown as solid lines and filled symbols, respectively.

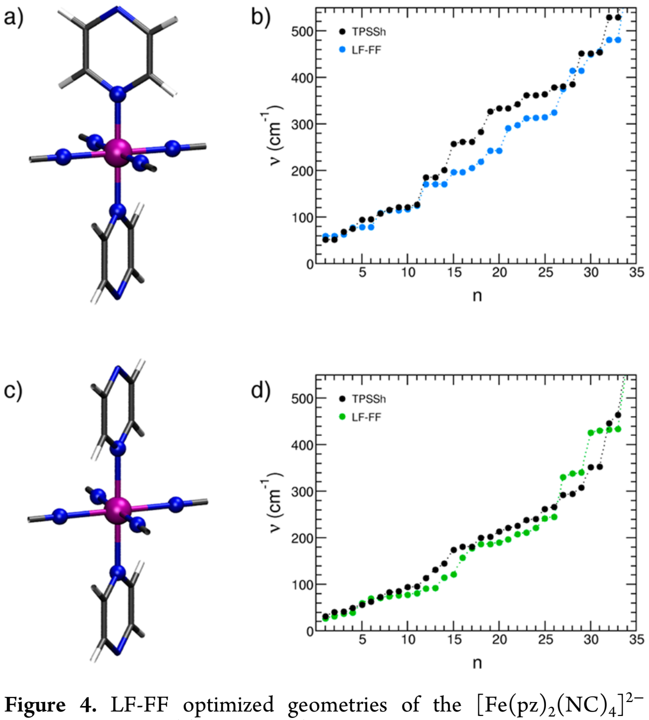

Figure 4. LF-FF optimized geometries of the $[Fe(pz)_2(NC)_4]^{2-}$ subunit in the LS (a) and HS (c) states. All atoms whose interactions are described through the LFMM parametrization are shown explicitly. Comparisons between the TPSSh (black) and the LF-FF computed harmonic frequencies below 500 cm^{-1} for the corresponding subunits in the (b) LS (blue) and (d) HS (green) states (n is the normal-mode index).

Supporting Information). Importantly, the LF-FFs developed in this study reproduce the correct stereochemistry of the pyrazine rings in each spin state, showing alternate and eclipsed configurations for the LS and HS states, respectively. Furthermore, the energy profiles calculated along the angular coordinate describing the rotation of the pyrazine ring about its principal symmetry axis show that the barriers predicted by the present LF-FFs are in close agreement with the corresponding TPSSh values (Figure S5 in the Supporting Information).

3.2. Calculation of Spin-Crossover Temperatures.

From a thermodynamic point of view, the SCO transition can be described as the thermal equilibrium between the LS and HS states:

$$\mathrm{LS} \leftrightarrows \mathrm{HS} \tag{4}$$

The free energy change (ΔG) associated with this equilibrium is then expressed as[68,69]

$$\Delta G = G^{\mathrm{HS}} - G^{\mathrm{LS}} = \Delta H - T\Delta S \tag{5}$$

where

$$G^i = H^i - TS^i = E^i_{\mathrm{el}} + E^i_{\mathrm{vib}} - TS^i \tag{6}$$

is the Gibbs free energy associated with spin state i. In eq 6, the enthalpy term (H^i) includes both electronic (E^i_{el}) and vibrational (E^i_{vib}) contributions. For molecular complexes, E^i_{vib} can be estimated using the harmonic approximation, while E^i_{el}, describing the electronic energy of spin state i, can be obtained directly from ab initio or LFMM calculations. The entropy contribution (S^i) can also be estimated within the harmonic approximation. Since at equilibrium $\Delta G = 0$, the SCO transition temperature ($T_{1/2}$) can be determined from

$$T_{1/2} = \frac{\Delta H}{\Delta S} \tag{7}$$

The equilibrium condition defined in eq 4 can also be expressed in terms of the equilibrium constant, K_{eq}:

$$\Delta G = -RT \ln K_{\mathrm{eq}} = -RT \ln \frac{\gamma_{\mathrm{HS}}}{1 - \gamma_{\mathrm{HS}}} \tag{8}$$

Equations 5 and 8 can thus be combined to determine γ_{HS}, which represents the relative population of the HS state at temperature T. Alternatively, the equilibrium populations of both LS and HS states at a given temperature can be determined directly from LFMM simulations carried out with the hybrid MC/MD approach described in the previous section. From the knowledge of the relative populations of the two spin states as a function of the temperature, it is possible to calculate the corresponding magnetic moment of the system within the spin-only approximation[70] and, consequently, to determine $T_{1/2}$ as the temperature at which $\gamma_{\mathrm{LS}} = \gamma_{\mathrm{HS}}$.

As a first application of our ab initio-based LF-FFs, the magnetic properties of the MOF building unit ($[Fe(pz)_2(NC)_4]^{2-}$) are investigated, which also serves as a direct test of the accuracy of the overall LFMM approach. Since no experimental data are currently available for the isolated SBU,

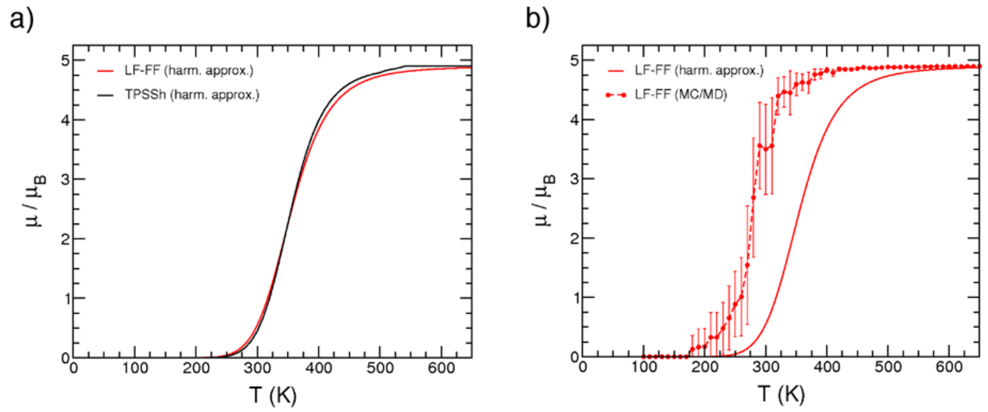

Figure 5. (a) Magnetization curves for the $[Fe(pz)_2(NC)_4]^{2-}$ SBU calculated within the harmonic approximation using TPSSh (solid black line) and LFMM (solid red line). (b) Comparison of the LFMM magnetization curves calculated within the harmonic approximation (solid red line) and from hybrid MC/MD simulations (dotted solid red line).

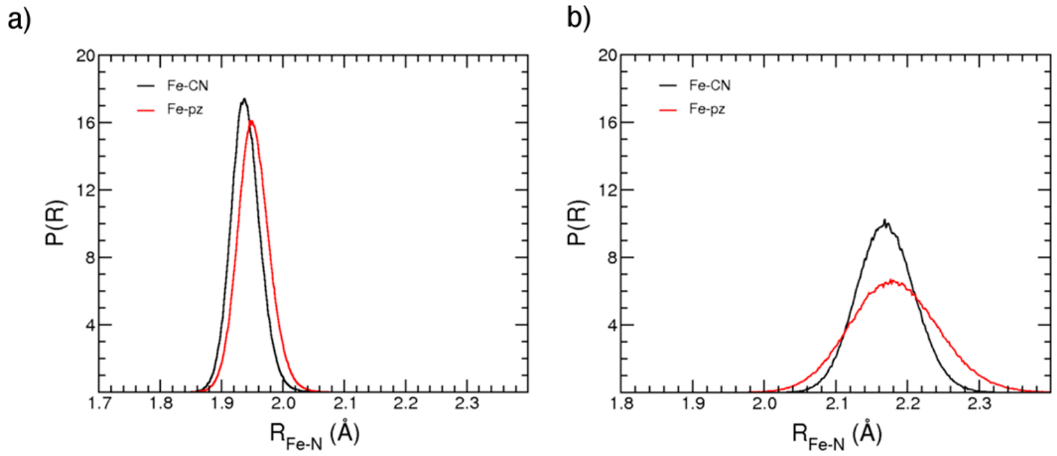

Figure 6. Probability distributions, $P(R)$, of Fe−N bonds (black line for Fe−CN and red line for Fe−pz) calculated for $[Fe(pz)_2(NC)_4]^{2-}$ in both LS (a) and HS (b) states. Each $P(R)$ was obtained from a 5 ns NVE trajectory at 400 K.

the temperature dependence of the magnetic moment of $[Fe(pz)_2(NC)_4]^{2-}$determined from the LFMM calculations is compared with the corresponding TPSSh results in Figure 5a. The LFMM normal-mode frequencies were obtained from the numerical diagonalization of the Hessian matrix calculated for the LF-FF optimized structures of the $[Fe(pz)_2(NC)_4]^{2-}$ SBU in both spin states. From eq 8, the TPSSh and LF-FF normal-mode frequencies were then used to compute the free-energy change between the LS and the HS states as a function of the temperature. The agreement between the LFMM and TPSSh results clearly demonstrates that the ab initio-based LF-FFs described in the previous section are capable of correctly representing the spin-state energy differences that arise from the different occupation of the d-based orbitals in each spin state as a function of thermally induced structural distortions.

The magnetization curve for the $[Fe(pz)_2(NC)_4]^{2-}$ SBU was also calculated directly from hybrid MC/MD simulations carried out at different temperatures. Specifically, sequential hybrid MC/MD simulations in the NVT ensemble were performed every 10 K, warming and cooling the system in the temperature range between 100 and 700 K. At each temperature, the magnetization was then calculated as the average between the two values, and the statistical uncertainty is given as the standard deviation. (The individual warming and cooling curves are shown in Figure S8 of the Supporting Information.) The results of the MC/MD simulations are compared with the corresponding TPSSh data in Figure 5b. The transition temperature predicted by the hybrid MC/MD simulations is ∼50 K (0.1 kcal/mol) lower than the corresponding value determined within the harmonic approximation. This difference can be explained by considering that the HS state is relatively "floppier" than the LS state (Figure S6 in the Supporting Information), which implies that anharmonic effects are more pronounced in the HS state than they are in the LS state. While these effects are neglected in the calculation of ΔG within the harmonic approximation, they are taken into account in the MC/MD simulations that effectively sample the relevant free-energy surface. Because anharmonic effects lead to an entropy increase of the system, it follows that the HS state becomes relatively more stable than the LS state. This results in a smaller energy gap between the LS and HS states and, consequently, in a lower transition temperature.

Because of the occupation of antibonding d_{z^2} and $d_{x^2-y^2}$ orbitals (see Supporting Information), the HS state of $[Fe(pz)_2(NC)_4]^{2-}$ is characterized by relatively weaker M−L bonds, which is reflected in broader distributions of the two Fe−N bond lengths calculated from NVE simulations carried out at 400 K (Figure 6). Interestingly, the analysis of the HS results shown in Figure 6 also indicates that the Fe−CN bond distribution is relatively narrower than the corresponding curve associated with the Fe−pz bond, which is a direct consequence of better bonding properties of CN^- with Fe(II) compared to pyrazine.

To investigate the SCO behavior of the $[Fe(pz)_2Pt(CN)_4]$ MOF, a series of MD simulations for the bulk material in both LS and HS states was initially carried out in the NσT ensemble by decreasing the temperature from 400 to 10 K. This procedure allowed the cell parameters to adapt to the corresponding equilibrium geometries, thus leading to the actual equilibrium structures for the two spin states at each temperature. These final configurations were then used to analyze the effects of the different orbital occupation on the bonding properties of the metal centers. The calculated average lengths of the equatorial and axial Fe−N bonds are 1.92 and 1.97 Å in the LS system and 2.15 and 2.27 Å in the HS system, respectively. These values are in good agreement with the crystallographic data reported for the $[Fe(pz)_2Pt(CN)_4]$ MOF in ref 21. Importantly, the MD simulations predict a larger length difference between the axial and equatorial bonds in the HS state, which, being consistent with the expectation based on the Jahn−Teller effect, demonstrates that the LF-FFs described in the previous section are capable of correctly representing electronically driven phenomena.

To calculate the transition temperature, 24 sequential 5 ns hybrid MC/MD simulations were carried out in the NσT ensemble at intervals of 25 K in the temperature range between 100 and 600 K. At each temperature, the total magnetic moment of the MOF material was calculated as

$$\mu_{\text{eff}} = \frac{n_{\text{HS}}\mu_{\text{HS}} + n_{\text{LS}}\mu_{\text{LS}}}{n_{\text{HS}} + n_{\text{LS}}} \tag{9}$$

where n_{LS} and n_{HS} are the average numbers of metal centers in the LS and HS states, respectively, and μ_{HS} and μ_{LS} are the corresponding magnetic moments estimated using the spin-only approximation for each spin state.[70] Assuming the validity of Curie's law, the magnetic moment is directly related to the product of the molar susceptibility and the temperature according to

$$\mu_{\text{eff}} \approx C\sqrt{\chi_{\text{M}}T} \tag{10}$$

Knowing μ_{eff} from eq 9, it is then possible to use eq 10 to determine $\chi_{\text{M}}T$ as a function of temperature. The comparison between the experimental and calculated $\chi_{\text{M}}T$ for the $[Fe(pz)_2Pt(CN)_4]$ MOF is shown in Figure 7. The hybrid MC/MD simulations predict a transition temperature of ~425 K, which is about 100 K higher than the experimental value (~306 K) measured during the warming process from the LS to the HS state. The shift of the SCO transition temperature of the bulk material to a higher value compared to that obtained for the isolated $[Fe(pz)_2(NC)_4]^{2-}$ subunit (Figure 5) can be understood by considering the collective nature of the vibrations in the MOF material with respect to its molecular counterpart. This shift in energy requires more thermal energy to excite the lattice vibrations that involve the Fe center and contribute the most to the SCO transition. It is interesting to note that the SCO transition in the MOF material takes place between 400 and 475 K, which is a significantly narrower interval than that calculated for the isolated $[Fe(pz)_2(NC)_4]^{2-}$ subunit (180 K < $T_{1/2}$ < 320 K). The hybrid MC/MD prediction for the bulk material is in good agreement with the available experimental data showing a sharp SCO transition extending for ~20 K.

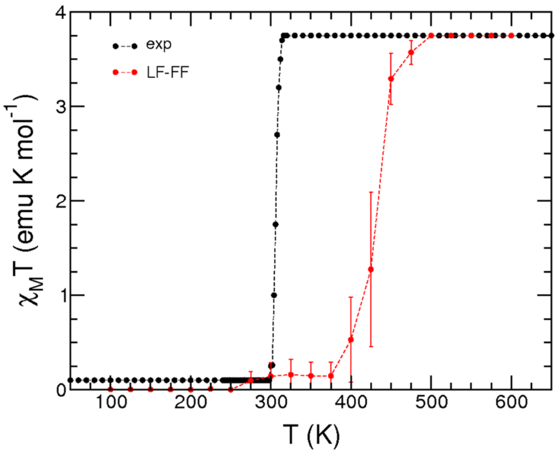

Figure 7. Comparison between the experimental (black) and calculated (red) $\chi_{\text{M}}T$ values for the $[Fe(pz)_2Pt(CN)_4]$ MOF. The experimental values are from ref 21.

4. SUMMARY AND OUTLOOK

The SCO behavior of $[Fe(pz)_2Pt(CN)_4]$, a MOF material that undergoes a transition from the LS to the HS state at approximately room temperature, was investigated using computer simulations. On the basis of our previous studies on molecular systems with SCO properties, a complete ligand-field force field for the MOF material was derived from ab initio data, including an accurate description of all possible spin states of the Pt (S = 0) and Fe (S = 0 and S = 2) centers. Building upon the LFMM methodology, the new LF-FF has been implemented in a novel hybrid Monte Carlo/molecular dynamics approach that has then been used to characterize the SCO properties of both the isolated $[Fe(pz)_2(NC)_4]^{2-}$ secondary building unit and the SCOF material. The new LF-FF correctly reproduces the potential energy surfaces associated with the two Fe(II) spin states of the secondary building unit and provides an accurate description of the corresponding normal modes. The SCO temperature for the $[Fe(pz)_2(NC)_4]^{2-}$ isolated complex calculated within the harmonic approximation using the new LF-FF is in excellent agreement with the value obtained from electronic structure calculations. Direct hybrid MC/MD simulations predict a slightly lower value for $T_{1/2}$, which is attributed to anharmonic effects that stabilize the HS state relatively more than the LS state.

The magnetization curve of the MOF material calculated from LF-FF simulations carried out with the hybrid MC/MD approach correctly reproduces the sharp transition between the LS and HS state observed experimentally, which is attributed to the collective nature of the framework vibrations. The hybrid MC/MD simulations for the MOF material predict a transition temperature between 400 and 475 K, which is in good agreement with the corresponding experimental value.

The hybrid MC/MD approach presented here can open the door to in silico screening of SCOF materials with targeted transition temperatures, providing fundamental molecular-level insights for the rational design of multifunctional materials. In this context, future work will focus on characterizing the effects that chemically and structurally different guest molecules can have on the SCO temperature.

■ ASSOCIATED CONTENT

Ⓢ Supporting Information

Optimized Cl−M−Cl angle for the $[MCl_4]^{2-}$ molecules (M^{2+} = Co, Ni, Cu) with our LFMM implementation compared with DFT values. Ab initio and LFMM harmonic frequencies, and potential energy scans for the $[Pt(CN)_4]^{2-}$ and $[Fe(pz)_2(NC)_4]^{2-}$ secondary building units. LF-FF parameters for both Pt(II) and Fe(II) centers. Magnetization curves for both the warming and cooling processes calculated for the $[Fe(pz)_2(NC)_4]^{2-}$ secondary building unit. Schematic molecular orbital diagrams for both LS and HS states of the $[Fe(pz)_2(NC)_4]^{2-}$ secondary building unit. Charge scheme and corresponding atom types used in the MD and hybrid MC/MD simulations. This material is available free of charge via the Internet at http://pubs.acs.org.

■ AUTHOR INFORMATION

Corresponding Author

*E-mail: fpaesani@ucsd.edu.

Author Contributions

The manuscript was written through contributions of all authors. All authors have given approval to the final version of the manuscript.

Notes

The authors declare no competing financial interest.

■ ACKNOWLEDGMENTS

We would like to thank Prof. R. J. Deeth for helpful discussions during the implementation of the electron−electron repulsion term. This work was supported by the U.S. Department of Energy, Office of Science, under Award No. DE-FG02-13ER16387, and used resources of the National Energy Research Scientific Computing Center, which is supported by the Office of Science of the U.S. Department of Energy under Contract No. DE-AC02-05CH11231.

■ REFERENCES

(1) Halcrow, M. A. *Spin-crossover materials: properties and applications;* John Wiley: Hoboken, NJ, 2013; p 564.

(2) Bousseksou, A.; Molnar, G.; Salmon, L.; Nicolazzi, W. *Chem. Soc. Rev.* **2011**, *40*, 3313.

(3) Gütlich, P.; Gaspar, A. B.; Garcia, Y. *Beilstein J. Org. Chem.* **2013**, *9*, 342.

(4) Hofmann, K. A.; Küspert, F. *Z. Anorg. Allg. Chem.* **1897**, *15*, 204.

(5) Yaghi, O. M.; Richardson, D. A.; Li, G.; Davis, C. E.; Groy, T. L. In *Open framework solids with diamond-like structures prepared from clusters and metal-organic building blocks,* Symposium on Advances in Porous Materials, MRS Fall Meeting, Boston, MA, Nov 28-Dec 01, 1994; Boston, Ma, Materials Research Society:Warrendale, PA, 1994; pp 15.

(6) Special Issue, *Chem. Soc. Rev.* **2009**, *38*, 1201.

(7) MacGillivray, L. R. *Metal-Organic Frameworks: Design and Application;* John Wiley & Sons, Inc.: Hoboken, NJ, 2010.

(8) Farrusseng, D. *Metal-Organic Frameworks;* Wiley-VCH Verlag & CO. KGaA: Weinheim, Germany, 2011; p 392.

(9) Bao, X.; Shepherd, H. J.; Salmon, L.; Molnar, G.; Tong, M.-L.; Bousseksou, A. *Angew. Chem., Int. Ed.* **2013**, *52*, 1198.

(10) Furukawa, H.; Cordova, K. E.; O'Keeffe, M.; Yaghi, O. M. *Science* **2013**, *341*, 974.

(11) Liu, J.; Thallapally, P. K.; McGrail, B. P.; Brown, D. R. *Chem. Soc. Rev.* **2012**, *41*, 2308.

(12) Suh, M. P.; Park, H. J.; Prasad, T. K.; Lim, D. W. *Chem. Rev.* **2012**, *112*, 782.

(13) Zhang, Q. F.; Uchaker, E.; Candelaria, S. L.; Cao, G. Z. *Chem. Soc. Rev.* **2013**, *42*, 3127.

(14) Deng, H.; Doonan, C. J.; Furukawa, H.; Ferreira, R. B.; Towne, J.; Knobler, C. B.; Wang, B.; Yaghi, O. M. *Science* **2010**, *327*, 846.

(15) Cohen, S. M. *Chem. Rev.* **2012**, *112*, 970.

(16) Tanabe, K. K.; Cohen, S. M. *Chem. Soc. Rev.* **2011**, *40*, 498.

(17) Kim, M.; Cahill, J. F.; Fei, H.; Prather, K. A.; Cohen, S. M. *J. Am. Chem. Soc.* **2012**, *134*, 18082.

(18) *Spin Crossover in Transition Metal Compounds I, II and III;* Springer: New York, 2004.

(19) Muñoz, M. C.; Real, J. A. *Coord. Chem. Rev.* **2011**, *255*, 2068.

(20) Muñoz Lara, F. J.; Gaspar, A. B.; Aravena, D.; Ruiz, E.; Carmen Munoz, M.; Ohba, M.; Ohtani, R.; Kitagawa, S.; Real, J. A. *Chem. Commun.* **2012**, *48*, 4686.

(21) Ohba, M.; Yoneda, K.; Agusti, G.; Carmen Munoz, M.; Gaspar, A. B.; Real, J. A.; Yamasaki, M.; Ando, H.; Nakao, Y.; Sakaki, S.; Kitagawa, S. *Angew. Chem., Int. Ed.* **2009**, *48*, 4767.

(22) Ohtani, R.; Yoneda, K.; Furukawa, S.; Horike, N.; Kitagawa, S.; Gaspar, A. B.; Carmen Munoz, M.; Real, J. A.; Ohba, M. *J. Am. Chem. Soc.* **2011**, *133*, 8600.

(23) Neville, S. M.; Halder, G. J.; Chapman, K. W.; Duriska, M. B.; Moubaraki, B.; Murray, K. S.; Kepert, C. J. *J. Am. Chem. Soc.* **2009**, *131*, 12106.

(24) Neville, S. M.; Halder, G. J.; Chapman, K. W.; Duriska, M. B.; Southon, P. D.; Cashion, J. D.; Letard, J.-F.; Moubaraki, B.; Murray, K. S.; Kepert, C. J. *J. Am. Chem. Soc.* **2008**, *130*, 2869.

(25) Halder, G. J.; Kepert, C. J.; Moubaraki, B.; Murray, K. S.; Cashion, J. D. *Science* **2002**, *298*, 1762.

(26) Real, J. A.; Andres, E.; Munoz, M. C.; Julve, M.; Granier, T.; Bousseksou, A.; Varret, F. *Science* **1995**, *268*, 265.

(27) Cirera, J.; Paesani, F. *Inorg. Chem.* **2012**, *51*, 8194.

(28) Jensen, K. P.; Cirera, J. *J. Phys. Chem. A* **2009**, *113*, 10033.

(29) Reiher, M. *Inorg. Chem.* **2002**, *41*, 6928.

(30) Reiher, M.; Salomon, O.; Hess, B. A. *Theor. Chem. Acc.* **2001**, *107*, 48.

(31) Burton, V. J.; Deeth, R. J. *J. Chem. Soc., Chem. Commun.* **1995**, 573.

(32) Burton, V. J.; Deeth, R. J.; Kemp, C. M.; Gilbert, P. J. *J. Am. Chem. Soc.* **1995**, *117*, 8407.

(33) Deeth, R. J. *Coord. Chem. Rev.* **2001**, *212*, 11.

(34) Deeth, R. J.; Anastasi, A.; Diedrich, C.; Randell, K. *Coord. Chem. Rev.* **2009**, *253*, 795.

(35) Deeth, R. J.; Fey, N.; Williams-Hubbard, B. *J. Comput. Chem.* **2005**, *26*, 123.

(36) Bureekaew, S.; Amirjalayer, S.; Tafipolsky, M.; Spickermann, C.; Roy, T. K.; Schmid, R. *Phys. Status Solidi B* **2013**, *250*, 1128.

(37) Maxim Tafipolsky, S. A. R. S. *J. Comput. Chem.* **2007**, *28*, 1169.

(38) Salles, F.; Ghoufi, A.; Maurin, G.; Bell, R. G.; Mellot-Draznieks, C.; Ferey, G. *Angew. Chem., Int. Ed.* **2008**, *47*, 8487.

(39) Devic, T.; Horcajada, P.; Serre, C.; Salles, F.; Maurin, G.; Moulin, B.; Heurtaux, D.; Clet, G.; Vimont, A.; Greneche, J. M.; Le Ouay, B.; Moreau, F.; Magnier, E.; Filinchuk, Y.; Marrot, J.; Lavalley, J. C.; Daturi, M.; Ferey, G. *J. Am. Chem. Soc.* **2010**, *132*, 1127.

(40) Salles, F.; Bourrelly, S.; Jobic, H.; Devic, T.; Guillerm, V.; Llewellyn, P.; Serre, C.; Ferey, G.; Maurin, G. *J. Phys. Chem. C* **2011**, *115*, 10764.

(41) Grosch, J. S.; Paesani, F. *J. Am. Chem. Soc.* **2012**, *134*, 4207.

(42) Schaffer, C. E.; Jorgense, C. K. *Mol. Phys.* **1965**, *9*, 401.

(43) Deeth, R. J.; Kemp, C. M. *J. Chem. Soc., Dalton Trans* **1992**, 2013.

(44) Gerloch, M.; Slade, R. C. *Ligand-Field Parameters;* Cambridge University Press: Cambridge, U.K., 1973; p 248.

(45) Allured, V. S.; Kelly, C. M.; Landis, C. R. *J. Am. Chem. Soc.* **1991**, *113*, 1.

(46) Deeth, R. J.; Anastasi, A. E.; Wilcockson, M. J. *J. Am. Chem. Soc.* **2010**, *132*, 6876.

(47) Anastasi, A. E.; Deeth, R. J. *J. Chem. Theory Comput.* **2009**, *5*, 2339.

(48) Bentz, A.; Comba, P.; Deeth, R. J.; Kerscher, M.; Seibold, B.; Wadepohl, H. *Inorg. Chem.* **2008**, *47*, 9518.
(49) Deeth, R. J.; Hearnshaw, L. J. A. *Dalton Trans.* **2006**, 1092.
(50) Todorov, I. T.; Smith, W.; Trachenko, K.; Dove, M. T. *J. Mater. Chem.* **2006**, *16*, 1911.
(51) Niel, V.; Thompson, A. L.; Munoz, M. C.; Galet, A.; Goeta, A. S. E.; Real, J. A. *Angew. Chem., Int. Ed.* **2003**, *42*, 3760.
(52) Ganzenmuller, G.; Berkaine, N.; Fouqueau, A.; Casida, M. E.; Reiher, M. *J. Chem. Phys.* **2005**, *122*.
(53) Handy, N. C.; Cohen, A. J. *Mol. Phys.* **2001**, *99*, 403.
(54) Lee, C. T.; Yang, W. T.; Parr, R. G. *Phys. Rev. B* **1988**, *37*, 785.
(55) Perdew, J. P.; Burke, K.; Ernzerhof, M. *Phys. Rev. Lett.* **1996**, *77*, 3865.
(56) Ye, S. F.; Neese, F. *Inorg. Chem.* **2010**, *49*, 772.
(57) Staroverov, V. N.; Scuseria, G. E.; Tao, J. M.; Perdew, J. P. *J. Chem. Phys.* **2003**, *119*, 12129.
(58) Kaneko, M.; Tokinobu, S.; Nakashima, S. *Chem. Lett.* **2013**, *42*, 1432.
(59) Frisch, M. J.; Trucks, G. W.; Schlegel, H. B.; Scuseria, G. E.; Robb, M. A.; Cheeseman, J. R.; Scalmani, G.; Barone, V.; Mennucci, B.; Petersson, G. A.; Nakatsuji, H.; Caricato, M.; Li, X.; Hratchian, H. P.; Izmaylov, A. F.; Bloino, J.; Zheng, G.; Sonnenberg, J. L.; Hada, M.; Ehara, M.; Toyota, K.; Fukuda, R.; Hasegawa, J.; Ishida, M.; Nakajima, T.; Honda, Y.; Kitao, O.; Nakai, H.; Vreven, T.; Montgomery, J., Jr.; Peralta, J. E.; Ogliaro, F.; Bearpark, M.; Heyd, J. J.; Brothers, E.; Kudin, K. N.; Staroverov, V. N.; Kobayashi, R.; Normand, J.; Raghavachari, K.; Rendell, A.; Burant, J. C.; Iyengar, S. S.; Tomasi, J.; Cossi, M.; Rega, N.; Millam, N. J.; Klene, M.; Knox, J. E.; Cross, J. B.; Bakken, V.; Adamo, C.; Jaramillo, J.; Gomperts, R.; Stratmann, R. E.; Yazyev, O.; Austin, A. J.; Cammi, R.; Pomelli, C.; Ochterski, J. W.; Martin, R. L.; Morokuma, K.; Zakrzewski, V. G.; Voth, G. A.; Salvador, P.; Dannenberg, J. J.; Dapprich, S.; Daniels, A. D.; Farkas, Ö.; Foresman, J. B.; Ortiz, J. V.; Cioslowski, J.; Fox, D. J. *Gaussian 09, Revision A.01 and C.01;* Gaussian, Inc.: Wallingford, CT, 2009.
(60) Schäfer, A.; Huber, C.; Ahlrichs, R. *J. Chem. Phys.* **1994**, *100*, 5829.
(61) Andrae, D.; Haussermann, U.; Dolg, M.; Stoll, H.; Preuss, H. *Theor. Chim. Acta* **1990**, *77*, 123.
(62) Halgren, T. A. *J. Comput. Chem.* **1996**, *17*, 490.
(63) Goldbert, D. E. *Genetic Algorithms in Search, Optimization, and Machine Learning*, 1st ed.; Addison-Wesley Longman Publishing Co., Inc: Boston, MA, 1989.
(64) Cundari, T. R.; Fu, W.; Moody, E. W.; Slavin, L. L.; Snyder, L. A.; Sommerer, S. O.; Klinckman, T. R. *J. Phys. Chem.* **1996**, *100*, 18057.
(65) Marques, H. M.; Munro, O. Q.; Grimmer, N. E.; Levendis, D. C.; Marsicano, F.; Pattrick, G.; Markoulides, T. *J. Chem. Soc., Faraday Trans.* **1995**, *91*, 1741.
(66) Deshmukh, M. M.; Ohba, M.; Kitagawa, S.; Sakaki, S. *J. Am. Chem. Soc.* **2013**, *135*, 4840.
(67) Frenkel, D.; Smit, B. *Understanding Molecular Simulations: From Algorithms to Simulations;* Elsevier: Academic Press: New York, 2001; Vol. *1*.
(68) Boča, R.; Linert, W. *Mon. Chem.* **2003**, *134*, 199.
(69) Gütlich, P.; Köppen, H.; Link, R.; Steinhäuser, H. G. *J. Chem. Phys.* **1979**, *70*, 3977.
(70) Kahn, O. *Molecular Magnetism;* VCH-Wiley: New York, 1993; p 396.